2013 American Control Conference (ACC)
Washington, DC, USA, June 17-19, 2013

Stability Analysis of a Tethered Airfoil

Sigitas Rimkus[1], Tuhin Das[1] and Ranjan Mukherjee[2]

***Abstract*— The stability analysis of a tethered airfoil system is presented and conditions required for the existence of stable equilibrium points are derived. Two cases are investigated: a case where the tether is assumed to be straight; and a second, more general case, where the tether is assumed to take a catenary geometry. For each case, the relevant equations of motion are derived and simulation results are used to validate the mathematical models. Specifically, for the straight tether case, the analytical conditions for stability are derived and simulated. For the catenary case, simulations were performed to investigate how the equilibrium point moves as operating conditions are varied.**

NOMENCLATURE

m_k	Mass of the airfoil
l_t, m_t	Length and mass of tether
l_e, m_e	Length and mass of each tether element
ϕ_k	Inclination of airfoil with horizontal
ϕ_i	Inclination of ith tether element with horizontal
y_n, z_n	y and z co-ordinates of position of nth tether element
$U_{\infty,y}$	Free stream air velocity component in y direction
$U_{\infty,z}$	Free stream air velocity component in z direction
$U_{rel,y}$	Relative velocity of wind in y direction
$U_{rel,z}$	Relative velocity of wind in z direction
U_{rel}	Free stream air velocity relative to airfoil
L, D	Lift and drag forces acting on the airfoil perpendicular and parallel to the direction of the velocity of the wind relative to the airfoil
F_c	Force on airfoil from tether
ρ	Free stream air density
C_L, C_D	Co-efficients of lift and drag
A	Airfoil area
α	Angle of attack
$\alpha_{L,0}$	Angle of attack for zero lift
ϵ	Span effectiveness factor
AR	Aspect Ratio
b, s	Wing span and wing area respectively
C_d	Profile drag
y_c, z_c	Co-ordinates of center of mass of airfoil
I_O	Moment of inertia for straight tether case

Subscripts:

e Values at equilibrium

[1]S. Rimkus and T. Das are with the Department of Mechanical and Aerospace Engineering, University of Central Florida, Orlando, FL 32816, USA(tdas@ucf.edu)

[2]R. Mukherjee is with the Department of Mechanical Engineering, Michigan State University, East Lansing, MI 48824, USA

INTRODUCTION

Machines used to convert the kinetic energy contained within wind into electrical power are becoming more and more commonplace. Arguably, the most popular type of these machines is the wind turbine which employs large rotating wings to generate electricity. However, a far more esoteric class of machines, consisting of tethered airfoils, used for power generation also exist. Machines like Ockels' "Laddermill" [1] and tether-airfoil design discussed in [2] have been described in literature. A small-scale test of a tethered airfoil system was described by Canale et al. [3] further validated the theory with experimental data. Work by Loyd [4] found that a kite of comparable size to a large airliner could produce more than 3 MW of power in a 10 m/s wind, a figure similar to that produced by a large wind turbine.

In their earlier work [5], the authors presented a simple model of a two-dimensional tether-airfoil system mounted on a base capable of linear horizontal motion. By oscillating the base in a particular manner and changing the angle of attack synchronously, useful power was generated. The authors also briefly presented an empirical method of determining the stability of the tether-airfoil system. By injecting small perturbations into the system in the form of step changes in wind velocity and intial conditions, the authors were able to show that the system tajectories converged to equilibrium.

In this paper, we investigate the stability problem of the tether-airfoil system. We consider two cases, a straight tether case, and a catenary tether case. The straight tether case is a good approximation of the tether shape for small tether lengths and high wind speed operating conditions where aerodynamic forces acting on the airfoil result in large tension forces in the tether. The catenary case is more general and is valid for lesser wind speeds. We first provide an overview outlining various assumptions and general aerodynamic equations which will allow for the derivation of the equations of motion for the straight tether and catenary geometry. Next, we derive the equations of motion and linearize them about the equilibrium point. Then, we provide the results of several simulations. Finally, we make concluding remarks.

SYSTEM DESCRIPTION AND MODEL DEVELOPMENT

Assumptions

We assume a tether-airfoil system as shown in Fig.1. For modeling the system, we make the following assumptions:

A1. The tether-airfoil system moves entirely within the yz-plane.

A2. The airfoil is a square, flat plate, and its instantaneous angle of attack α is sufficiently small that the the foil is not in a stalled condition.
A3. The tether is negligibly thin, inextensible, and is not subject to aerodynamic loads.
A4. The velocity of the oncoming wind has time-steady magnitude and direction.
A5. A control system is used to maintain a constant inclination ϕ_k of the airfoil, i.e. $\dot{\phi}_k = 0$.
A6. The tether is connected to a stationary base O.

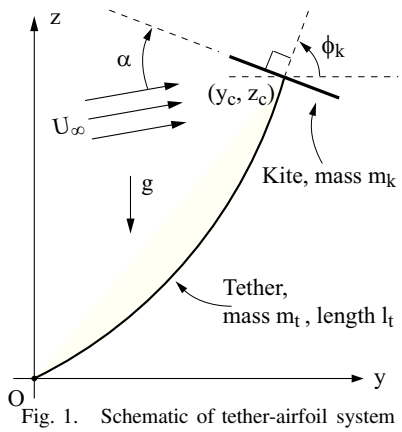

Fig. 1. Schematic of tether-airfoil system

Forces on the Airfoil: Lift and Drag Formulation

A free body diagram of the airfoil is shown in Fig.2. For the sake of conciseness, the net moment on the airfoil due to external forces is not shown since it assumed that $\dot{\phi}_k = 0$ through an active control, assumption A5. The lift and drag

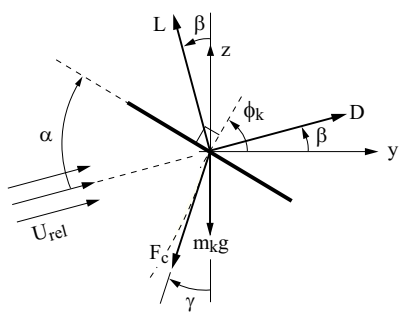

Fig. 2. Free-body Diagram of Airfoil

forces acting on the airfoil are

$$L = \frac{1}{2}\rho C_L A||\vec{U}_{rel}||^2, \quad D = \frac{1}{2}\rho C_L A||\vec{U}_{rel}||^2 \tag{1}$$

where

$$||\vec{U}_{rel}||^2 = U_{rel,y}^2 + U_{rel,z}^2, \quad \tan\beta = U_{rel,z}/U_{rel,y}$$

The calculation of C_L and C_D are described in detail in [5], which are based on *thin airfoil theory* discussed in [6], [7]. The lift coefficient is modeled as

$$C_L(\alpha) = \frac{dC_L}{d\alpha}(\alpha - \alpha_{L,0}), \ \frac{dC_L}{d\alpha} = \frac{2\pi}{1 + \frac{2}{\epsilon AR}}, \ AR = \frac{b^2}{s} \tag{2}$$

where ϵ is obtained from experimental data, and with typical values in the range $0.8 \leq \epsilon \leq 1$. The drag coefficients is modeled as

$$C_D = C_d(\alpha) + \frac{C_L^2(\alpha)}{\pi\epsilon AR} \tag{3}$$

STABILITY ANALYSIS

Location of Static Equilibrium Point

At static equilibrium, the forces on the tether are shown in Fig.3. From Figs.2 and 3, and using subscript e to represent

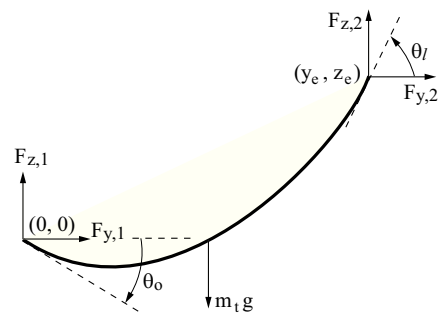

Fig. 3. Tether with Forces at Equilibrium

equilibrium condition, we have

$$D_e \cos\beta_e - L_e \sin\beta_e = F_{y,2} \tag{4}$$
$$D_e \sin\beta_e + L_e \sin\beta_e - m_k g = F_{z,2}. \tag{5}$$

where (y_e, z_e) is the static equilibrium position of the center of mass of the airfoil. From force balance at equilibrium configuration of the tether, we obtain

$$F_{y,1} = -F_{y,2}, \quad F_{z,1} = m_t g - F_{z,2} \tag{6}$$

At equilibrium, the tether takes the shape of a *catenary*, with equation

$$z = a\cosh\left(\frac{y-q}{a}\right) + h \tag{7}$$

where h, q and a are constant parameters of the catenary. The length of the tether is constant and from Eq.(7)

$$\begin{aligned} l_t &= \int_0^{y_e} \sqrt{1 + \left(\frac{dz}{dy}\right)^2}\, dy \\ &= a\left(\sinh\left(\frac{y_e - q}{a}\right) - \sinh\left(-\frac{q}{a}\right)\right). \end{aligned} \tag{8}$$

We also note in Fig.3, that the tension at any point of the catenary is directed tangential to the catenary. Hence,

$$\begin{aligned} -\frac{dz}{dy}|_{(0,0)} = \tan\theta_0 &= \sinh\left(-\frac{q}{a}\right) = \frac{-F_{z,1}}{F_{y,1}} \\ \frac{dz}{dy}|_{(y_e,z_e)} = \tan\theta_l &= \sinh\left(\frac{y_e - q}{a}\right) = \frac{F_{z,2}}{F_{y,2}} \end{aligned} \tag{9}$$

Noting that L_e and D_e can be calculated for a steady operating condition and noting that $\tan\beta_e = U_{\infty,z}/U_{\infty,z}$, the above equations can be solved to calculate the static equilibrium position (y_e, z_e).

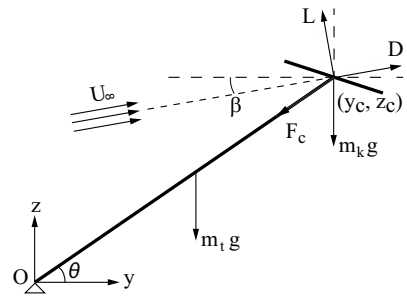

Fig. 4. Straight Tether-airfoil with External Forces

Stability Analysis with Straight Tether Assumption

The straight tether assumption can be valid at high wind speeds when the tether tension is high. We apply this assumption to derive simple analytical conditions for stability. The assumption also reduces the tether-airfoil to a 1DOF system. For straight tether, $y_c = l_t \cos\theta$ and $z_c = l_t \sin\theta$, and the equation of motion in θ can be written as

$$I_O\ddot{\theta} = l_t L\cos(\theta-\beta) - l_t D\sin(\theta-\beta) \tag{10}$$

$$-\left(m_k + \frac{m_t}{2}\right) g l_t \cos\theta,\ I_O = \left(\frac{1}{3}m_t + m_k\right) l_t^2 \tag{11}$$

The formulations of the lift force L and drag force D are

$$L = \frac{1}{2}\rho C_L A\left[2U_\infty^2 + 2U_\infty l_t\dot{\theta}(\sin\theta - \cos\theta) + l_t^2\dot{\theta}^2\right]$$
$$D = \frac{1}{2}\rho C_D A\left[2U_\infty^2 + 2U_\infty l_t\dot{\theta}(\sin\theta - \cos\theta) + l_t^2\dot{\theta}^2\right] \tag{12}$$

respectively, where β is

$$\beta = \arctan\left(\frac{U_{\infty,z} - \dot{z}}{U_{\infty,y} - \dot{y}}\right) = \arctan\left(\frac{U_{\infty,z} - l_t\dot{\theta}\cos\theta}{U_{\infty,y} + l_t\dot{\theta}\sin\theta}\right) \tag{13}$$

In order to investigate the stability of the static equilibrium, we linearize Eq.(11) about the equilibrium angle θ_e

$$I_O\ddot{\delta} = f(\theta_e, 0) + \left.\frac{\partial f}{\partial\theta}\right|_{\theta_e,0}\delta + \left.\frac{\partial f}{\partial\dot{\theta}}\right|_{\theta_e,0}\dot{\delta} \tag{14}$$

where $\delta = \theta - \theta_e$, and $f(\theta_e, \dot{\theta_e})$ is the right-hand side of Eq.(11). Carrying out the derivatives and grouping like terms yields the linearized equation of motion

$$I_O\ddot{\delta} + c\dot{\delta} + k\delta = 0 \tag{15}$$

where

$$c = \left[\frac{1}{2}\rho A l_t^2 C_D U_\infty\left(1 + \sin^2(\theta_e - \beta_e)\right)\right.$$
$$\left.-\frac{1}{2}\rho A l_t^2 C_L U_\infty \cos(\theta_e - \beta_e)\sin(\theta_e - \beta_e)\right] \tag{16}$$

$$k = \left[\frac{1}{2}\rho A l_t C_D U_\infty^2 \cos(\theta_e - \beta_e) - \left(m_k + \frac{m_t}{2}\right) g l_t \sin\theta_e\right.$$
$$\left.-\frac{1}{2}\rho A l_t C_L U_\infty^2 \sin(\theta_e - \beta_e)\right] \tag{17}$$

For the above second order linear system, the necessary and sufficient conditions for stable equilibrium at $\theta = \theta_e$ are $I_O > 0$, $c > 0$, and $k > 0$. The inertia I_O is always positive, so the inequality conditions for the coefficients c and k determine stability. Evaluating the inequality condition for c yields

$$\frac{C_D}{C_L} > \frac{\cos(\theta_e - \beta_e)\sin(\theta_e - \beta_e)}{1 + \sin^2(\theta_e - \beta_e)} \tag{18}$$

Similarly, evaluating the inequality condition for k yields

$$C_D\cos(\theta_e - \beta_e) - C_L\sin(\theta_e - \beta_e) > \frac{(2m_k + m_t)g}{\rho A U_\infty^2}\sin\theta_e \tag{19}$$

Stability Analysis with Catenary Tether

In this section, we will relax the straight tether assumption and instead consider the tether to retain the catenary shape for small perturbations about the equilibrium. This amounts to using a statics based model for the catenary while studying the dynamic behavior of the tether-airfoil system close to equilibrium. Now we have a 2DOF system since y_c and z_c can change independently as long as the tether length l_t remains unchanged. The equations of motion are

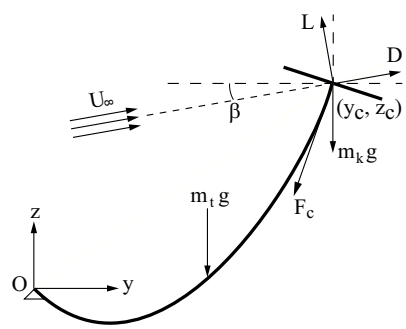

Fig. 5. Catenary Tether-Airfoil with External Forces

$$m_k\ddot{y}_c = D\cos\beta - L\sin\beta - F_{c,y} \tag{20}$$
$$m_k\ddot{z}_c = D\sin\beta + L\cos\beta - F_{c,z} - m_k g \tag{21}$$

We linearize the equations of motion about the equilibrium point (y_e, z_e)

$$m_k\delta\ddot{y} = \left.\frac{\partial D\cos\beta}{\partial\dot{y}}\right|_e\delta\dot{y} + \left.\frac{\partial D\cos\beta}{\partial\dot{z}}\right|_e\delta\dot{z} - \left.\frac{\partial L\sin\beta}{\partial\dot{y}}\right|_e\delta\dot{y}\cdots$$
$$-\left.\frac{\partial L\sin\beta}{\partial\dot{z}}\right|_e\delta\dot{z} - \left.\frac{\partial F_{c,y}}{\partial y}\right|_e\delta y - \left.\frac{\partial F_{c,y}}{\partial z}\right|_e\delta z \tag{22}$$

and

$$m_k\delta\ddot{z} = \left.\frac{\partial D\sin\beta}{\partial\dot{y}}\right|_e\delta\dot{y} + \left.\frac{\partial D\sin\beta}{\partial\dot{z}}\right|_e\delta\dot{z} + \left.\frac{\partial L\cos\beta}{\partial\dot{y}}\right|_e\delta\dot{y}\cdots$$
$$+\left.\frac{\partial L\cos\beta}{\partial\dot{z}}\right|_e\delta\dot{z} - \left.\frac{\partial F_{c,z}}{\partial y}\right|_e\delta y - \left.\frac{\partial F_{c,z}}{\partial z}\right|_e\delta z \tag{23}$$

where $\delta y = y - y_e$ and $\delta z = z - z_e$ and $|_e$ represents calculation at the equilibrium. Carrying out the derivatives for the aerodynamic forces in Eq.(22) using Eq.(13), and

noting in Fig.2 that $\alpha - \beta + \phi_k = \frac{\pi}{2}$ yields

$$\begin{aligned} m_k \delta\ddot{y} = & \frac{1}{2}\rho A \left[C_L U_{\infty,z} \cos\beta_e - C_D \left(\frac{U_{\infty,y}^2 + U_\infty^2}{U_\infty} \right) \cdots \right. \\ & \left. + U_{\infty,z} \left(\cos\beta_e \frac{dC_D}{d\alpha}\bigg|_e - \sin\beta_e \frac{dC_L}{d\alpha}\bigg|_e \right) \right] \delta\dot{y} \cdots \\ & + \frac{1}{2}\rho A \left[C_L \left(\frac{U_{\infty,z}^2 + U_\infty^2}{U_\infty} \right) - C_D U_{\infty,z} \cos\beta_e \cdots \right. \\ & \left. + U_{\infty,y} \left(-\cos\beta_e \frac{dC_D}{d\alpha}\bigg|_e + \sin\beta_e \frac{dC_L}{d\alpha}\bigg|_e \right) \right] \delta\dot{z} \cdots \\ & - \frac{\partial F_{c,y}}{\partial y}\bigg|_e \delta y - \frac{\partial F_{c,y}}{\partial z}\bigg|_e \delta z \end{aligned} \tag{24}$$

Performing the same steps on Eq.(23) yields

$$\begin{aligned} m_k \delta\ddot{z} = & -\frac{1}{2}\rho A \left[C_L \left(\frac{U_{\infty,y}^2 + U_\infty^2}{U_\infty} \right) + C_D U_{\infty,z} \cos\beta_e \cdots \right. \\ & \left. + U_{\infty,z} \left(\sin\beta_e \frac{dC_D}{d\alpha}\bigg|_e + \cos\beta_e \frac{dC_L}{d\alpha}\bigg|_e \right) \right] \delta\dot{y} \cdots \\ & - \frac{1}{2}\rho A \left[C_L U_{\infty,z} \cos\beta_e + C_D \left(\frac{U_{\infty,z}^2 + U_\infty}{U_\infty} \right) \cdots \right. \\ & \left. - U_{\infty,y} \left(\sin\beta_e \frac{dC_D}{d\alpha}\bigg|_e + \cos\beta_e \frac{dC_L}{d\alpha}\bigg|_e \right) \right] \delta\dot{z} \cdots \\ & - \frac{\partial F_{c,z}}{\partial y}\bigg|_e \delta y - \frac{\partial F_{c,z}}{\partial z}\bigg|_e \delta z \end{aligned} \tag{25}$$

where, in Eqs.(24) and (25)

$$\frac{dC_L}{d\alpha}\bigg|_e = \frac{2\pi}{1 + \frac{2}{eAR}}, \quad \frac{dC_D}{d\alpha}\bigg|_e = \left(\frac{dC_d}{d\alpha} + \frac{2C_L}{\pi e AR} \frac{dC_L}{d\alpha} \right)\bigg|_e \tag{26}$$

are obtained from Eqs.(2) and (3). To solve the spatial derivatives of $F_{c,y}$ and $F_{c,z}$, we proceed as follows. We first note from Eq.(7) that

$$\cosh\left(\frac{q}{a}\right) = -\frac{h}{a}, \quad z_e = \cosh\left(\frac{y_e - q}{a}\right) + h \tag{27}$$

Upon differentiation and rearranging Eqs.(27) and (8),

$$\mathbf{A} \begin{bmatrix} da \\ dq \\ dh \end{bmatrix} = \mathbf{B} \begin{bmatrix} \delta y \\ \delta z \end{bmatrix} \tag{28}$$

where $\mathbf{A} \in \mathbb{R}_{3\times3}$ and $\mathbf{B} \in \mathbb{R}_{3\times2}$. The entries for $\mathbf{A}$ are

$$\begin{aligned} & a_{11} = -\left[q \sinh\left(\frac{q}{a}\right) + h \right], \qquad a_{12} = a \sinh\left(\frac{q}{a}\right) \\ & a_{21} = \left(\frac{y_e - q}{a}\right) \sinh\left(\frac{y_e - q}{a}\right) - \cosh\left(\frac{y_e - q}{a}\right) \\ & a_{22} = \sinh\left(\frac{y_e - q}{a}\right) \\ & a_{31} = \frac{l_t}{a} - \frac{q}{a}\cosh\left(\frac{q}{a}\right) - \left(\frac{y_e - q}{a}\right)\cosh\left(\frac{y_e - q}{a}\right) \\ & a_{32} = \cosh\left(\frac{q}{a}\right) - \cosh\left(\frac{y_e - q}{a}\right) \\ & a_{13} = a, \qquad a_{23} = -1, \qquad a_{33} = 0 \end{aligned} \tag{29}$$

and the entries for $\mathbf{B}$ are

$$\begin{aligned} & b_{11} = 0, \quad b_{12} = 0, \quad b_{21} = \sinh\left(\frac{y_e - q}{a}\right), \quad b_{22} = -1 \\ & b_{31} = -\cosh\left(\frac{y_e - q}{a}\right), \qquad b_{32} = 0 \end{aligned} \tag{30}$$

From Eqs.(6) and (9) we have

$$dF_{z,1} = -dF_{z,2}, \quad dF_{y,1} = -dF_{y,2} \tag{31}$$

Now, for a small change in the catenary, the corresponding change in slope and tension forces at $(0,0)$ can be related as

$$d\left(\frac{dz}{dy}\right)\bigg|_{(0,0)} = \frac{F_{z,1} + dF_{z,1}}{F_{y,1} + dF_{y,1}}, \tag{32}$$

which upon simplification yields

$$\begin{aligned} \frac{F_{z,1} + dF_{z,1}}{F_{y,1} + dF_{y,1}} &= \frac{F_{z,1}}{F_{y,1}} - \frac{1}{a}\cosh\left(\frac{-q}{a}\right) \begin{bmatrix} \frac{-q}{a} & 1 & 0 \end{bmatrix} \begin{bmatrix} da \\ dq \\ dh \end{bmatrix} \\ &= \frac{F_{z,1}}{F_{y,1}} - \mu \mathbf{M}\mathbf{A}^{-1}\mathbf{B} \begin{bmatrix} \delta y \\ \delta z \end{bmatrix} \\ &= \frac{F_{z,1}}{F_{y,1}} - p\delta y - q\delta z \end{aligned} \tag{33}$$

Equation (33) can be expressed as

$$\begin{bmatrix} F_{z,1} \\ -F_{y,1} \end{bmatrix}^T \begin{bmatrix} dF_{y,2} \\ dF_{z,2} \end{bmatrix} = -F_{y,1}^2 \begin{bmatrix} p \\ q \end{bmatrix}^T \begin{bmatrix} \delta y \\ \delta z \end{bmatrix} \tag{34}$$

Taking a similar approach for (y_e, z_e) yields

$$\begin{bmatrix} -F_{z,2} \\ F_{y,2} \end{bmatrix}^T \begin{bmatrix} dF_{y,2} \\ dF_{z,2} \end{bmatrix} = -F_{y,2}^2 \begin{bmatrix} u - \nu \\ v \end{bmatrix}^T \begin{bmatrix} \delta y \\ \delta z \end{bmatrix} \tag{35}$$

where,

$$\nu = \frac{1}{a}\cosh\left(\frac{y_e - q}{a}\right), \ \mathbf{N} = \begin{bmatrix} \frac{y_e - q}{a} & 1 & 0 \end{bmatrix}, \tag{36}$$

and u and v are defined as

$$\nu \mathbf{N}\mathbf{A}^{-1}\mathbf{B} \left[\delta y \ \ \delta z\right]^T = u\delta y + v\delta z \tag{37}$$

Combining Eqs.(34) and (35) we get

$$\left[\partial F_{c,y} \ \ \partial F_{c,z}\right]^T = \left[\partial F_{y,2} \ \ \partial F_{z,2}\right]^T = \mathbf{Q}^{-1}\mathbf{U} \left[\partial y \ \ \partial z\right]^T \tag{38}$$

where

$$\mathbf{Q} = \begin{bmatrix} F_{z1} & -F_{y1} \\ -F_{z2} & F_{y2} \end{bmatrix}, \ \mathbf{U} = \begin{bmatrix} -pF_{y1}^2 & -qF_{y1}^2 \\ -(u-\nu)F_{y2}^2 & -vF_{y2}^2 \end{bmatrix}. \tag{39}$$

When assembled as a matrix equation, Eqs.(24) and (25) take the form

$$\begin{bmatrix} m_k & 0 \\ 0 & m_k \end{bmatrix} \begin{bmatrix} \delta\ddot{y} \\ \delta\ddot{z} \end{bmatrix} + \mathbf{C} \begin{bmatrix} \delta\dot{y} \\ \delta\dot{z} \end{bmatrix} + \mathbf{K} \begin{bmatrix} \delta y \\ \delta z \end{bmatrix} = 0 \tag{40}$$

The matrix $\mathbf{C}$ consists solely of terms from aerodynamic forces, and $\mathbf{K}$ consists of terms related to the tension in the tether. For stability, the eigenvalues of the matrix

$$\begin{bmatrix} \mathbf{0} & \mathbf{I}_{2\times 2} \\ -\mathbf{M}^{-1}\mathbf{K} & -\mathbf{M}^{-1}\mathbf{C} \end{bmatrix} \tag{41}$$

must have negative real parts. Solving for the eigenvalues of Eq.(41) analytically is tedious and hence we resort to numerical computations to generate a root-locus, shown in the next section.

Simulations and Observations

Before presenting the simulation results, the specific formulae for C_L and C_D developed for this model are given. We assume a square shaped wing span with one of the corners facing the head wind. For a square of side a, from Eq.(2) $AR = (\sqrt{2}a)^2/a^2 = 2$. The parameter ϵ is taken as 0.8 and $\alpha_{L,0}$ as -0.035rad ($\approx 2°$) based on experimental data from various NACA airfoils presented in [6], [7], [5]. This yields

$$C_L = 2.793(\alpha + 0.035) \tag{42}$$

The profile drag C_d was obtained from [8], based on the range of Reynolds numbers expected for wind speeds varying from 10 m/s to 30 m/s. The resulting drag coefficient is

$$C_D = 0.1943\alpha^2 + 0.00625 + 0.199C_L^2 \tag{43}$$

Stability Conditions: Straight Tether Assumption

Table I shows the parameters used in simulating the airfoil's operation. Our preliminary estimates of the total

TABLE I
SIMULATION PARAMETERS

Parameter	Value
l_t	100 m
m_t	0.5 kg
m_k	2 kg
A	2 m^2
I_O	2.5 $\mathrm{kg}\cdot\mathrm{m}^2$
ρ	1.3 $\mathrm{kg}\cdot\mathrm{m}^{-3}$
$U_{y,i}$	15 $\mathrm{m}\cdot\mathrm{s}^{-1}$
$U_{y,f}$	20 $\mathrm{m}\cdot\mathrm{s}^{-1}$
$n+1$	10

tether drag, assuming it to be a vertical cylinder, is $\leq$ 5N even with a conservative estimate of the tether diameter (assuming a tether made of Kevlar). Hence, we assert that the negligible tether drag assumption is plausible, [8]. Using the same numerical as in [5], a simulation is run for 300 seconds with the step wind change from $U_{y,i}$ to $U_{y,f}$ occurring at 200 seconds. The results of the simulation are shown in Fig. 6. As shown in Fig. 6(a), the average tether angle ϕ_i ranges from about 1.34 radians before the step change to about 1.45 radians after the step change. The tight bands of ϕ_i values indicate a high level of tension within the tether. Referring to Eq.(18) and Fig. 6(e), there are two values of θ_e to consider, namely $\theta_e = \tan^{-1}(97.3/22.9) = 1.3399$ rads, and $\theta_e = \tan^{-1}(99.2/12.5) = 1.4455$ rads.

The calculated ratio and the simulated ratio of C_D to C_L are both shown in Fig.7(a). The calculated ratio is found using Eq.(18) and the values for θ_e mentioned above. The

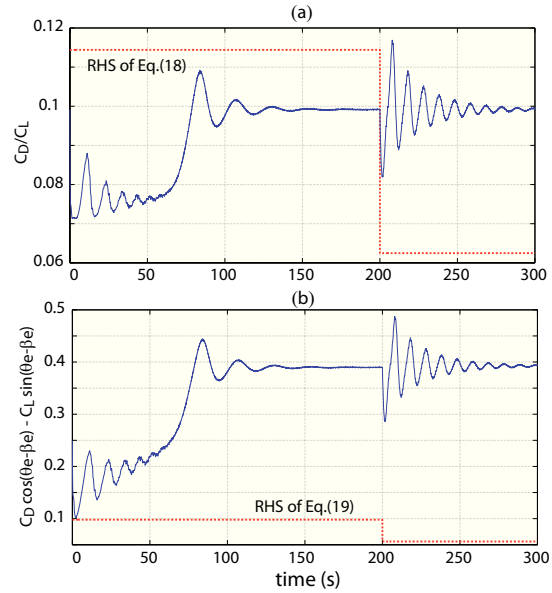

Fig. 7. Verifying Stability Criteria from Straight Tether Assumption

value of θ_e is assumed to change instantaneously with the step wind change. The simulated ratio is found using the simulated values of C_D and C_L at each time step. As shown in Fig.7(a), for the first 200 seconds of simulation, the first stability criterion defined by Eq.(18) is violated, yet the equilibrium is stable. However, once the wind speed is increased, the stability criterion is satisfied. The second stability criterion comes from Eq.(19) and is represented graphically in Fig.7(b). In this case, the second stability criterion is satisfied at all times. The above results show the validity of the straight tether assumption at higher wind speeds.

Stability Conditions: Catenary

As mentioned earlier, the catenary model represents a more accurate geometric configuration of the tether under steady state operating conditions. Fig. 8 graphically illus-

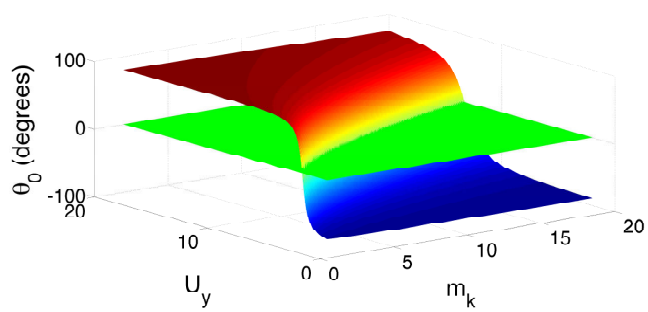

Fig. 8. Equilibrium Tether Angles for Varying U_y and m_k

trates the equilibrium angle θ_0 for a range of wind speeds U_y and airfoil mass m_k. The angle θ_0 represents the angle made by the tether with the horizontal at the base $(0, 0)$. The plot confirms the expected result that as the mass increases and/or the wind speed reduces, the equilibrium point transitions

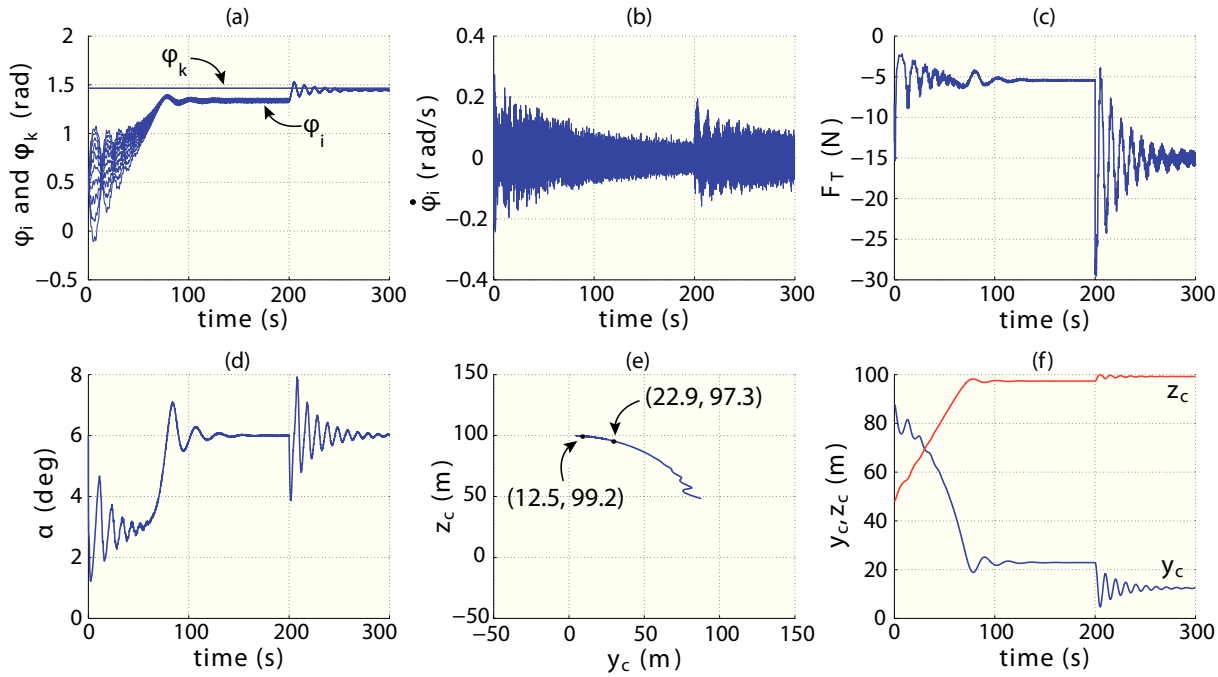

Fig. 6. Response to Step Change in Wind Speed

from one with positive altitude to one with negative altitude. Recall that solving for the eigenvalues of Eq.(41) will provide insight to the stability of a given equilibrium point. We next generate the root locus plot where, in Fig.9(a) the wind speed U_y is held constant and the airfoil mass m_k is varied over a range. In Fig.9(b), the airfoil mass m_k was chosen to be 2kg,

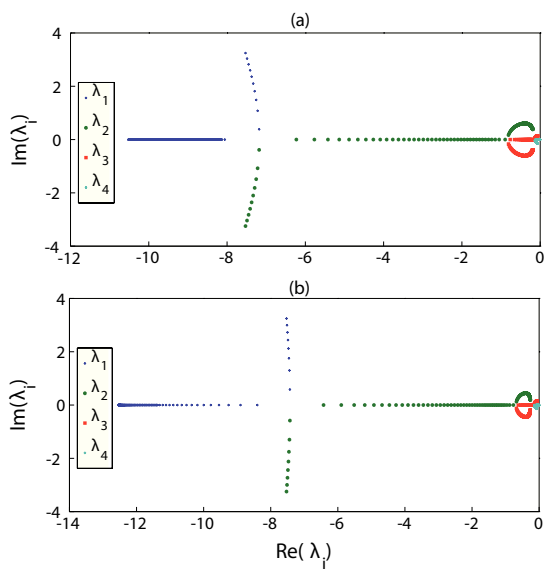

Fig. 9. Root Locus from Catenary Tether Model (a) Varying m_k and (b) Varying U_y

and the wind speed U_y was varied. All of the eigenvalues shown in Fig. 9 have negative real parts, thus indicating that the static equilibrium points are stable.

Conclusion

A stability analysis for a tether-airfoil has been presented, and conditions for the existence of stable equilibria have been investigated. For a straight tether, an assumption that would be valid for high wind speeds, analytical conditions for stability were derived and confirmed through simulations. Since the tether length and weight can be substantial, the tether model was refined to that of a catenary. A statics based model of the catenary was augmented to the dynamic model of the airfoil, to perform a more realistic study of stability. For the latter case, stability of equilibrium points for varying wind speed and varying airfoil mass were verified numerically. Future work will include analyzing stability when the tether-airfoil system is used for harnessing wind energy. Also, a linearization approach, which gives necessary and sufficient conditions for stability, cannot be used to detect periodic orbits, such as crosswind flight. Future work will investigate the nonlinear behavior of the system.

References

[1] W.J. Ockels. Laddermill, a novel concept to exploit the energy in the airspace. *Aircraft Design*, 4(81-97), 2001.
[2] P. Willams, B. Lansdorp, and W. Ockels. Optimal cross-wind towing and power generation with tethered kites. *AIAA Journal of Guidance, Control and Dynamics*, 31, 2008.
[3] M. Canale, L. Fagiano, and M. Milanese. High altitude wind energy generation using controlled power kites. *IEEE Transactions on Control Systems Technology*, 18 (2):279–293, 2010.
[4] M.L. Loyd. Crosswind kite power. *Journal of Energy*, 4 (3):106–111, 1980.
[5] T. Das, R. Mukherjee, , R. Sridhar, and A. Hellum. Two dimensional modeling and simulation of a tethered airfoil system for harnessing wind energy. *ASME Dynamic Systems and Control Conference*, 2011.
[6] J. D. Anderson Jr. *Fundamentals of Aerodynamics*. McGraw-Hill, 2010.
[7] J. D. Anderson Jr. *Introduction to Flight*. McGraw-Hill, 2011.
[8] F.M. White. *Fluid Mechanics*. McGraw-Hill, 2002.